Nano Scale Disruptive Silicon-Plasmonic Platform for Chip-to-Chip Interconnection

D 3.1 - Report on studies of optimized structure for metallic/plasmonic nano-laser and its coupling to Si-waveguide

Deliverable no.:	D3.1
Due date:	10/31/2012
Actual Submission date:	11/05/2012
Authors:	TUE
Work package(s):	WP3
Distribution level:	RE[1] (NAVOLCHI Consortium)
Nature:	document, available online in the restricted area of the NAVOLCHI webpage

List of Partners concerned

Partner number	Partner name	Partner short name	Country	Date enter project	Date exit project
1	Karlsruher Institut für Technologie	KIT	Germany	M1	M36
2	INTERUNIVERSITAIR MICRO-ELECTRONICA CENTRUM VZW	IMEC	Belgium	M1	M36
3	TECHNISCHE UNIVERSITEIT EINDHOVEN	TU/e	Netherlands	M1	M36
4	RESEARCH AND EDUCATION LABORATORY IN INFORMATION TECHNOLOGIES	AIT	Greece	M1	M36
5	UNIVERSITAT DE VALENCIA	UVEG	Spain	M1	M36
6	STMICROELECTRONICS SRL	ST	Italy	M1	M36
7	UNIVERSITEIT GENT	UGent	Belgium	M1	M36

[1] **PU** = Public
PP = Restricted to other programme participants (including the Commission Services)
RE = Restricted to a group specified by the consortium (including the Commission Services)
CO = Confidential, only for members of the consortium (including the Commission Services)

Deliverable Responsible

Organization: Eindhoven University of Technology
Contact Person: Victor Dolores-Calzadilla
Address: Faculty of Electrical Engineering
P.O. Box 513
5600 MB Eindhoven
The Netherlands
Phone: +31 (0) 40247 5129
E-mail: v.calzadilla@tue.nl

Executive Summary

The design and optimization of two metal-cavity lasers with electrical injection and coupled to a dielectric waveguides are described in this report. The optical performance of a Fabry Perot plasmonic laser and a metallo-dielectric nanolaser are investigated with FDTD (Finite-Difference Time-Domain) simulations. The results show that a metallo-dielectric nanolaser offers several advantages over a plasmonic laser. The mode in this laser has a lower optical loss because it is mainly confined in the semiconductor rather than in the metal, but its mode volume remains low due to the metal confinement. Additionally, it promises room temperature operation and high differential quantum efficiency with a threshold current below 100 μA. In view of the predicted performance of the metallo-dielectric nanolaser presented, it has been decided to carry out its fabrication to provide the NAVOLCHI project with a sub-micron laser source.

Change Records

Version	Date	Changes	Author
0.1 (draft)	2012-02-11		V. Calzadilla, M. Smit
1 (submission)	2012-05-11		V. Calzadilla, M. Smit

1. Introduction

It is the aim of WP3 to develop a laser with a metallic cavity coupled to a silicon waveguide. This report describes the design of a plasmonic and a metallo-dielectric laser, both coupled to an InP waveguide. For technological feasibility reasons, the laser is coupled as a first step to an InP waveguide on a silicon substrate. The coupling to a Si-waveguide will be done in a second stage, by tapering the InP-based waveguide to couple the optical mode down to an underlying Si waveguide. This approach to integrate III-V active devices with silicon waveguides has been recently demonstrated [1].

This report is organized as follows: in section 2, the design of a Fabry Perot plasmonic laser is reported. Section 3 describes the optimization of a metallo-dielectric nanolaser, and finally, in section 4, the conclusions of this deliverable are presented.

2. Plasmonic Fabry Perot laser

2.1. Device structure

The laser structure proposed is shown in Fig. 1, which is based on previously reported plasmonic lasers [2]. The laser consists fundamentally of a MISIM (metal-insulator-semiconductor-insulator-metal) waveguide forming a Fabry Perot resonator coupled to a dielectric waveguide, fabricated on an InP-membrane. The top n-contact and the lateral p-type contact provide the electrical pumping for the InGaAs active medium, which has a bandgap of $1.65\ \mu m$.

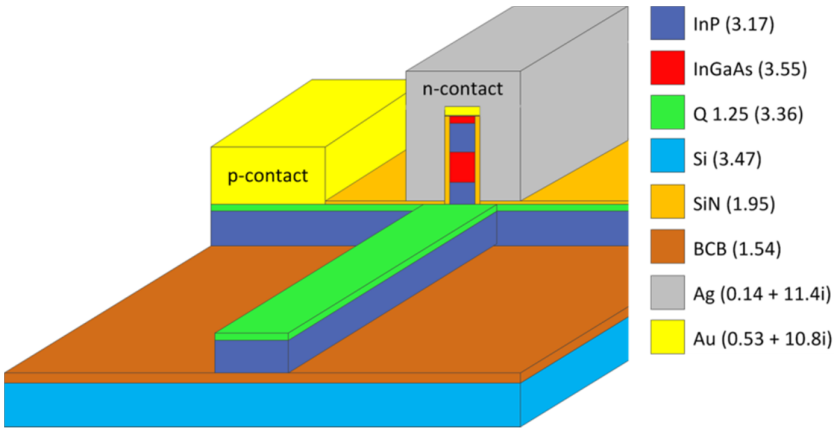

Figure 1. Schematic representation of a plasmonic laser coupled to a dielectric waveguide. The refractive index of each material at $1.55\ \mu m$ is shown in parenthesis. Optical absorption in InGaAs has been neglected for the simulations.

As it can be seen in Fig. 1, there is a thin insulating layer of SiN between the semiconductor layer stack and the metal cladding, which serves to insulate the structure horizontally and therefore allow a top-down current flow. The quaternary (Q 1.25) layer acts as the ohmic contact layer for the p-contact. The back side of the Fabry Perot cavity is completely terminated by metal to achieve a strong reflection, whereas it has an open facet at the frontal end to improve the

coupling. To estimate the threshold material gain $g_{th}$of this structure, we calculate the propagation loss α, the confinement factor Γ, and the facet reflectivities R_1 and R_2. Lasing in a cavity with length L is achieved when

$$g_{th}\Gamma = \alpha + \frac{1}{2L} ln\left(\frac{1}{R_1 R_2}\right). \quad (1)$$

2.2. Modal properties

The intensity distribution of the hybrid surface plasmon polariton mode with lowest loss in the cavity is shown in Fig. 2b. Due to its plasmonic nature, it has a dominant E_x component and is mainly confined within the insulation layer, which leads to a very poor overlap with the active region. The post height h is important because it influences the reflectivity and the coupling efficiency.

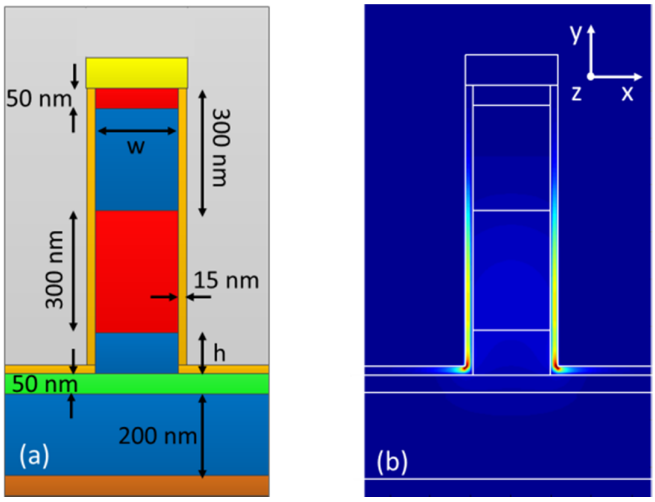

Figure 2. (a) Cross section of the plasmonic laser cavity with the dimensions used for the simulations. (b) Optical intensity of the plasmonic mode at 1.55 μm. Blue: low intensity. Red: high intensity.

The propagation loss and confinement factor as a function of the width w, can be observed in Fig. 3 for different values of the post height h. This loss is due to the absorption by the metal and it decreases when the core is wider because the mode is increasingly confined in the core. An increase in the width of the MISIM structure also leads to a higher confinement factor. The confinement factor is defined as the ratio of the electric field square amplitude within the active medium divided by to the square of the total electric field amplitude and, therefore, determines the modal gain.

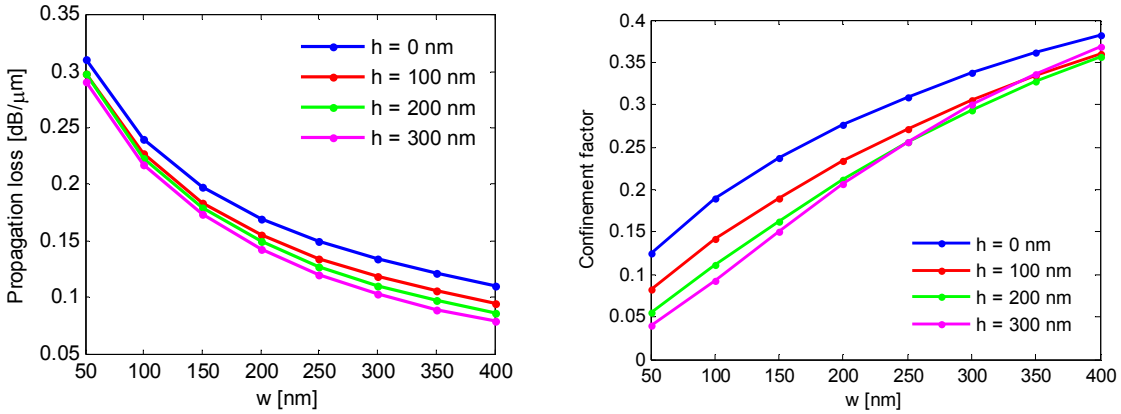

Figure 3. Left : Propagation loss due to the optical absorption of the metal cladding as a function of post width w. Right: Confinement factor in the active region as a function of post width w. The calculations were performed for a wavelength of 1.55 μm.

As can be seen in Fig. 3, a wider MISIM structure leads to a lower propagation loss and a higher confinement factor, however dielectric modes with better characteristics could exist for such wide structures and then the lasing mode will not be plasmonic anymore. Therefore, we have fixed the width to 200 nm. This is believed to be near the minimum width for a structure to be able to operate at room temperature, although using long cavities exceeding several tens of microns are necessary as discussed below.

2.3. Facet reflectivity and laser efficiency

Figure 4 shows the facet reflectivity and coupling efficiency as a function of wavelength for an open facet and different post heights (colored curves). The first remarkable characteristic is the high reflectivity of around 0.6 at 1.55 μm, which is twice the Fresnel reflectivity for an interface given by InGaAs and air, considering perpendicular incidence. This strong reflection is due to the large effective mode index mismatch between surface plasmon modes and free propagating modes in air.

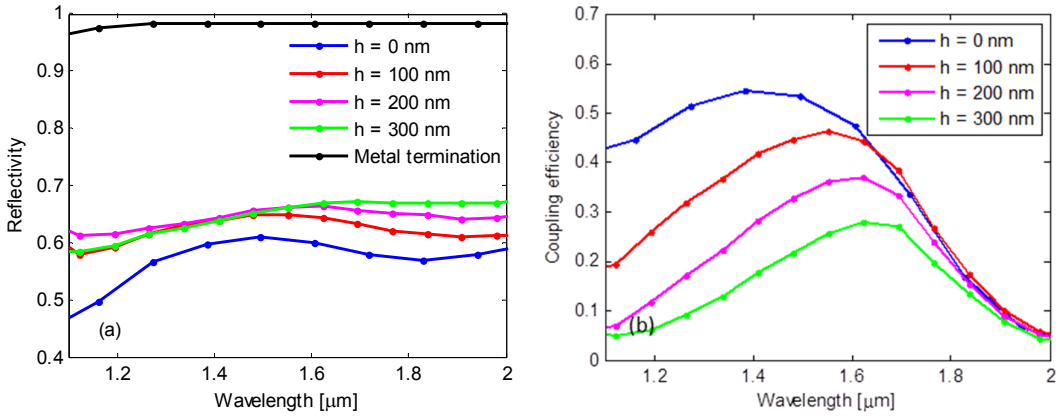

Figure 4. (a) Reflectivity of a laser structure with $w = 200\ nm$, for an open facet with post height h and a metal termination with $h = 0\ nm$. (b) Coupling efficiency of a laser structure with $w = 200\ nm$.

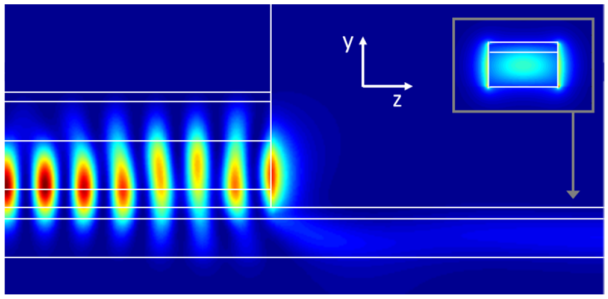

Figure 5. Longitudinal cross section showing the coupling between the laser and the dielectric waveguide. The inset shows a transversal cross section of the waveguide. Blue: low intensity. Red: high intensity. The plot shows the modulus squared of the electric field.

In addition, the reflectivity at the backside of the laser, which is assumed to have a metal coating, is shown in black in Fig. 4a. As expected, it is above 95% and nearly independent of h. The reflectivity increases only about 0.1 when increasing the post height because it is limited by the reflection between the laser structure and air. On the other hand, the coupling efficiency continuously decreases with increasing post height. Since the primary interest is to design an efficient laser, a post height of $100\,nm$ would be suitable for an operating wavelength of $1.55\,\mu m$, since it maximizes the reflectivity without compromising the outcoupling. Using a higher post would lead to a decrease in the laser efficiency. Figure 5 shows the intensity distribution of the coupling between the laser and the dielectric waveguide.

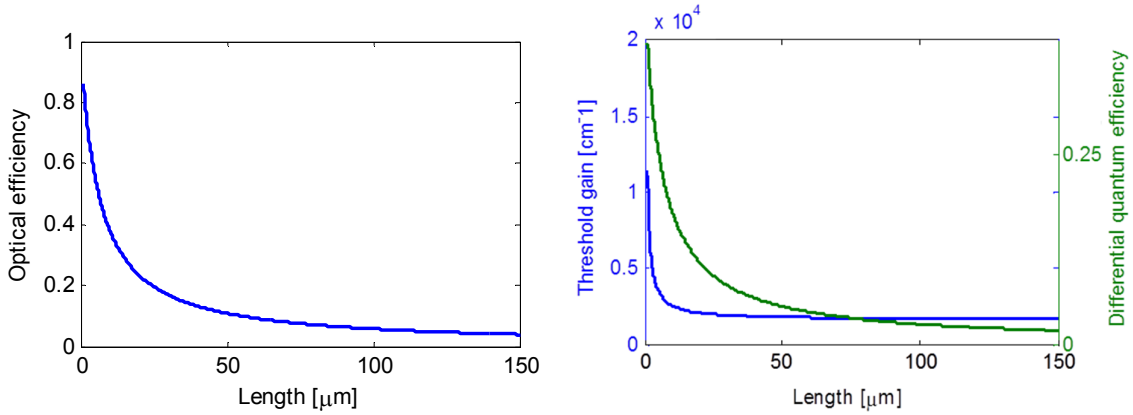

Figure 6. Left : Optical efficiency calculated as the mirror loss divided by the total loss of the cavity. Right: Threshold gain and differential quantum efficiency assuming unity internal quantum efficiency.

Given the modal and cavity properties presented above, it is possible to calculate the threshold gain with Eq. (1). Figure 6 shows both, optical and differential quantum efficiencies, as well as the threshold gain required to overcome losses. For example, assuming a laser length of $50\,\mu m$ and considering a cavity with $w = 200\,nm$ and $h = 100\,nm$, it gives $\alpha = 0.16\ dB/\mu m$, $\Gamma = 0.23$, $R_1 = 0.65$ and $R_2 = 0.98$, resulting in a threshold gain of $g_{th} = 1796\,cm^{-1}$ with only 5% of differential quantum efficiency, which is possible at room temperature under a high injected carrier density above $6 \cdot 10^{18}\ cm^{-3}$ [3].

3. Metallo-dielectric nanolaser

3.1. Introduction

In this section, the design of a metallo-dielectric laser with higher performance is presented. The combination of dielectric and metallic confinement can lead to strong optical confinement of a dielectric mode with relatively low loss, and has been used to demonstrate room-temperature lasing in a subwavelength cavity [4]. However, efficient coupling to a waveguide has not been demonstrated yet. In Ref. [5] the coupling of a III-V metallo-dielectric nanopillar laser to a Si/SiO_2 waveguide was proposed. In this report, a metallo-dielectric cavity laser coupled to a waveguide on a III-V membrane bonded with BCB to silicon is described and studied.

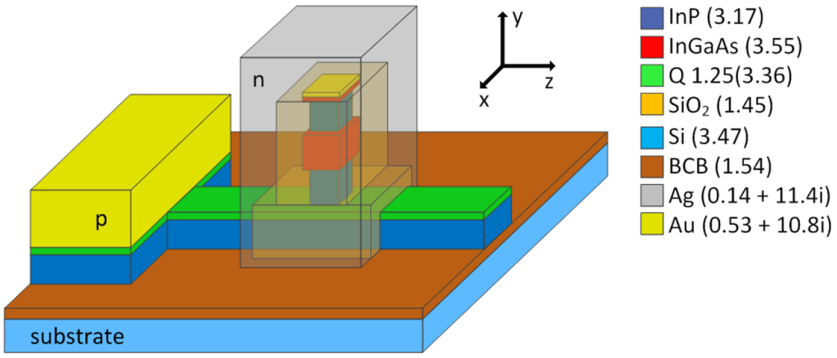

Figure 7. Model of the metallo-dielectric laser coupled to an InP-membrane waveguide. The refractive index of each material at $1.55\ \mu m$ is shown in parenthesis.

The proposed laser structure is shown in Fig. 7. The semiconductor laser pillar lies on top of a thin InP waveguide and it is insulated with a SiO_2 layer from a metallic cladding. A lateral p-contact is electrically connected to the pillar through a highly p-doped quaternary (InGaAsP) layer. The metallic cladding acts itself as the n-contact allowing a top-down current flow. For simplicity, Fig. 7 does not show the ohmic contact layers Ti/Pt/Au, however they were included in the simulation model in order to account for their optical loss.

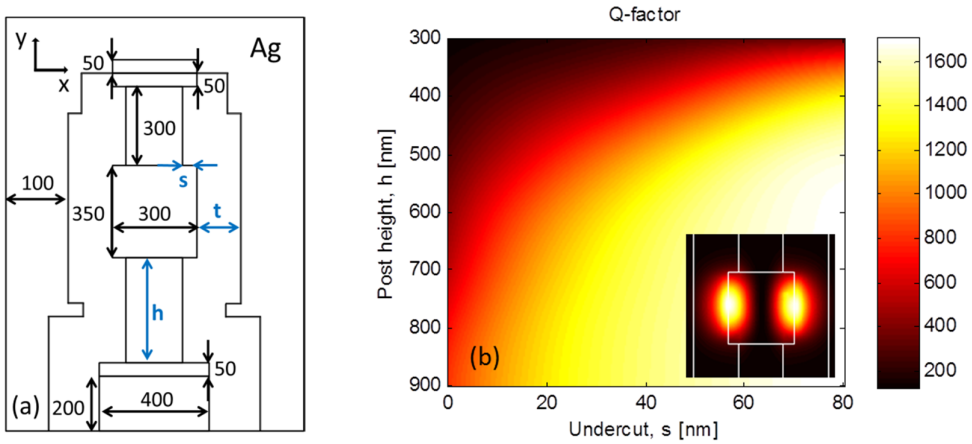

Figure 8. (a) Schematic of the cavity with dimensions in nanometers. The optimization parameters are shown in blue. (b) Q-factor as a function of undercut and post height for an insulation thickness $t = 175\ nm$. The inset shows the modulus squared of the electric field distribution of the TE polarized mode in the xy plane across the center of the cavity.

3.2. Quality factor and coupling properties

For the optimization of the insulation thickness t of the cavity, a bottom post height $h = 700\ nm$ was initially considered, since it provides sufficient isolation from the waveguide as suggested in Fig. 8b. Additionally, the pillar laser is considered to be symmetric along x and z (i.e. the length and width of the active medium are both $300\ nm$). For a thin insulation layer, metal losses are high, whereas the radiation losses increase for a thick insulation. Therefore, there is an optimum insulation thickness ($t = 175\ nm$) where the Q-factor is maximum as can be seen in Fig. 9a. The resonant wavelength for this thickness is around $1.4\ \mu m$, nevertheless it will be shown later that this can be increased to $1.55\ \mu m$ by changing the aspect ratio of the cavity.

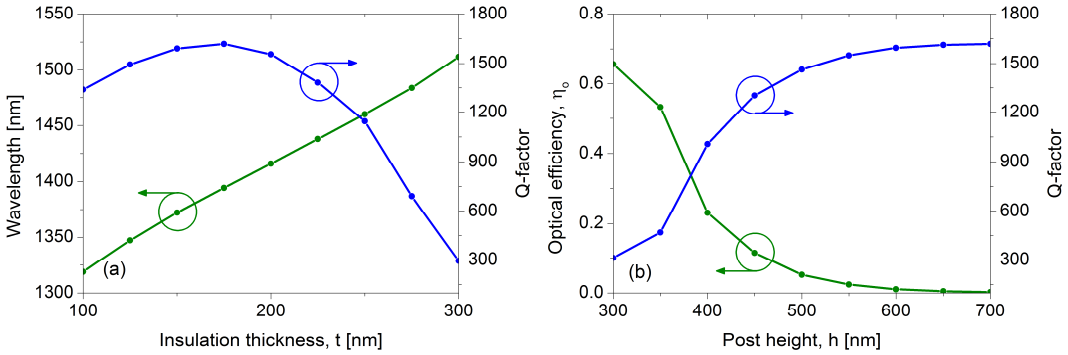

Figure 9. (a) Q-factor and resonant wavelength as a function of the insulation thickness, considering $h = 700\ nm$. (b) Q-factor and optical efficiency for a varying bottom post height, considering $t = 175\ nm$.

Once the optimum insulating thickness has been found, the bottom post height is varied in order to increase the coupling to the waveguide. The total loss rate in this nanopillar laser can be written as the sum $\gamma_{total} = \gamma_{metal} + \gamma_{sub} + \gamma_{wg}$, describing the loss into the metal, the radiation

into the substrate and the useful coupling to the waveguide, respectively [5]. We define the optical efficiency of the cavity as $\eta_o = (\gamma_{sub} + \gamma_{wg})/\gamma_{total}$ (ratio of total radiated power to total lost power). Its dependence on the post height is shown in Fig. 9b. As expected, the optical efficiency increases at the expense of the Q-factor when decreasing the post height.

A symmetric cavity has been considered until now, however the coupling efficiency can be increased by breaking the symmetry of the cavity, which can be realized by elongating the cavity in the z-direction [5]. The coupling efficiency η_c is defined as the ratio between the power coupled to the waveguide (in both directions) and the total radiated power: $\eta_c = \gamma_{wg}/(\gamma_{sub} + \gamma_{wg})$. Figure 10 shows an increase in coupling efficiency and resonant wavelength for an elongated cavity, while the Q-factor decreases. The desired lasing wavelength of 1.55 μm is achieved for a cavity length of 400 nm.

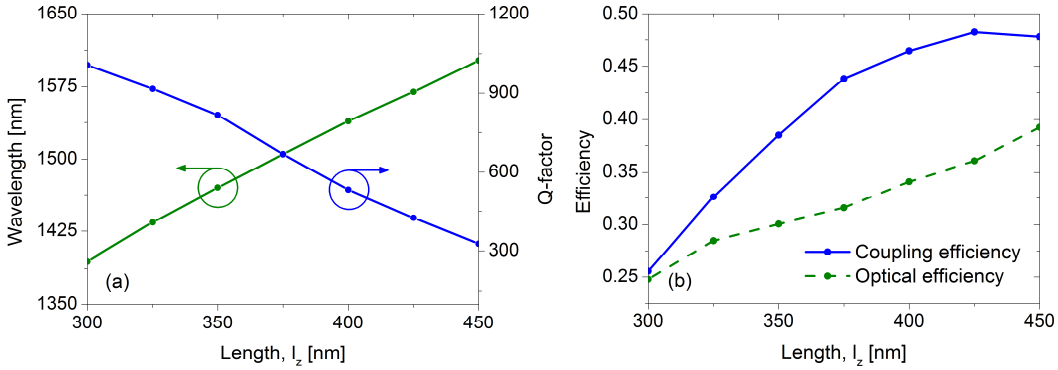

Figure 10. (a) Q-factor and resonant wavelength for an elongated cavity with active medium length l_z. (b) Improvement of optical and coupling efficiencies by elongating the cavity. Both graphs consider $t = 175\ nm$ and $h = 400\ nm$.

3.3. Differential efficiency and threshold conditions

The differential quantum efficiency determines the final amount of optical power coupled to the waveguide, and it is given by $\eta_d = \eta_o \eta_c$, assuming a unity internal quantum efficiency. Figure 11a shows the differential efficiency and the threshold gain of the asymmetric cavity. The threshold gain is calculated as $g_{th} = 2\pi n_g/Q\Gamma\lambda_0$, where n_g is the group velocity of the active medium, Q is the cavity quality factor, Γ is the confinement factor and λ_0 is the resonant wavelength in vacuum. According to our simulations, the confinement factor in the cavity varies almost linearly from 0.4 to 0.28 for a cavity length varying from 300 nm to 450 nm. As a result, Fig. 11 shows that the metallo-dielectric laser studied offers a much better performance than the previously proposed waveguide-coupled plasmonic laser within the NAVOLCHI project[6].

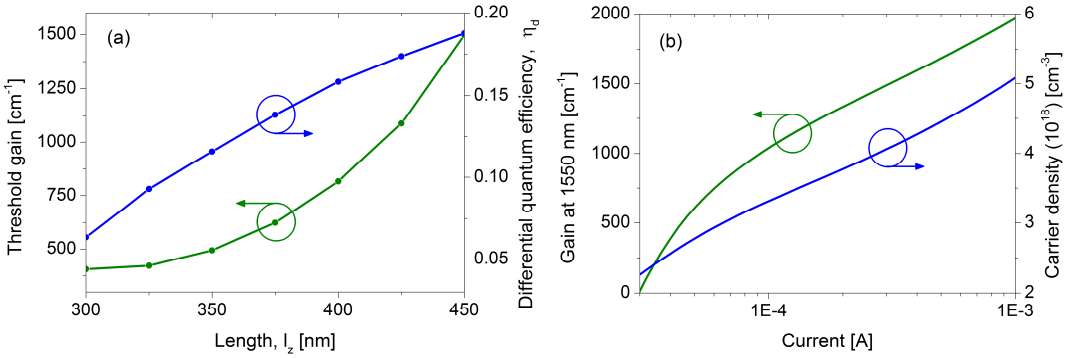

Figure 11. (a) Lasing threshold gain and differential quantum efficiency as a function of the cavity length. (b) Material gain of InGaAs and carrier density as a function of injection current.

Finally, Fig. 11b shows gain-current calculations performed in order to estimate the threshold current expected in the proposed laser device. The material gain curve was calculated from the transition matrix element and assuming parabolic bands [7], and the carrier density was calculated with a 2D self-consistent Poisson solver.

4. Conclusions

Despite the relatively large propagation loss and low confinement factor of the plasmonic laser presented in section two, such a structure is interesting in view of the high reflectivity at its open facet and coupling to a dielectric waveguide mode. The threshold gain can be compatible with room temperature operation for long structures (several tens of micrometers), albeit with a poor efficiency and at high carrier densities. Shorter structures can be realizable at room temperature, however they require to be wider to support dielectric modes with high confinement factor and lower metal loss, as it is the case in the metallo-dielectric lasers.

The design of a metallo-dielectric laser operating near $1.55\ \mu m$ coupled to a thin InP waveguide has been presented in section three. The influence of the main structural parameters was studied to optimize its performance. The optimized cavity has an insulation thickness of $175\ nm$ to maximize the Q-factor, a bottom post height of $400\ nm$ and a cavity length of $400\ nm$ to provide a high differential efficiency. This results in a low threshold gain of $815\ cm^{-1}$, which can be reached with a current injection of about $70\ \mu A$ at room temperature. Due to the better performance of the metallo-dielectric nanolaser compared to the plasmonic laser, we have decided to continue with the fabrication of this laser.

References

[1] S. Keyvaninia, *et* al., "Heterogeneously integrated III-V/Si multi-wavelength laser based on a ring resonator array multiplexer", accepted as postdeadline paper for ACP Conference, 2012.

[2] M. T. Hill: Status and prospects for metallic and plasmonic nano-laser, J. Opt. Soc. Am. B, 27(11), pp. 36-44, 2010.

[3] C. Y. Lu, , *et al.*, "A surface-emitting 3D metal-nanocavity laser: proposal and theory", Optics express, 19(14), pp. 13225-44, 2011.

[4] M. P. Nezhad, *et al.*, "Room-temperature subwavelength metallo-dielectric lasers", Nature Photonics, 4(4), pp. 395–399, 2010.

[5] M. K. Kim, *et* al., "Efficient waveguide-coupling of metal-clad nanolaser cavities", Optics express, 19(23), pp. 23504–12, 2011.

[6] V. Dolores-Calzadilla, *et al.*, "Towards plasmonic lasers for optical interconnects", IEEE Proceedings of the 14th International Conference on Optical Transparent Networks, 2012.

[7] L. A. Coldren, *et al.*, "Diode lasers and photonic integrated circuits", John Wiley & Sons, 2nd edition, 2012.